THE JOURNAL OF PHYSICAL CHEMISTRY LETTERS
A JOURNAL OF THE AMERICAN CHEMICAL SOCIETY

pubs.acs.org/JPCL Letter

Solvation Behavior of Elastin-like Polypeptides in Divalent Metal Salt Solutions

Yani Zhao,[‖] Swaminath Bharadwaj,[‖] Ryan L. Myers,[‖] Halil I. Okur, Pho T. Bui, Mengrui Cao, Lauren K. Welsh, Tinglu Yang, Paul S. Cremer,* and Nico F. A. van der Vegt*

Cite This: *J. Phys. Chem. Lett.* 2023, 14, 10113−10118 Read Online

ACCESS | Metrics & More | Article Recommendations | Supporting Information

ABSTRACT: The effects of $CaCl_2$ and $MgCl_2$ on the cloud point temperature of two different elastin-like polypeptides (ELPs) were studied using a combination of cloud point measurements, molecular dynamics simulations, and infrared spectroscopy. Changes in the cloud point for the ELPs in aqueous divalent metal cation solutions were primarily governed by two competing interactions: the cation−amide oxygen electrostatic interaction and the hydration of the cation. In particular, Ca^{2+} cations can more readily shed their hydration shells and directly contact two amide oxygens by the formation of ion bridges. By contrast, Mg^{2+} cations were more strongly hydrated and preferred to partition toward the amide oxygens along with their hydration shells. In fact, although hydrophilic ELP $V_5A_2G_3$ was salted-out at low concentrations of $MgCl_2$, it was salted-in at higher salt concentrations. By contrast, $CaCl_2$ salted the ELP sharply out of solution at higher salt concentrations because of the bridging effect.

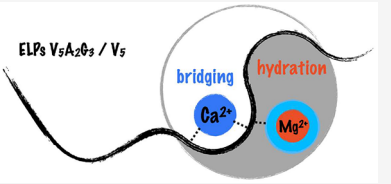

The phase behavior of macromolecules in aqueous solutions can be modulated by salts through a combination of ion−ion, ion−water, and macromolecule−water (hydration shell) interactions.[1−6] Although the dominant effect of salts has been attributed to anion effects, a direct cationic Hofmeister series has been proposed for the salting-out of proteins from aqueous solutions:[7−10] $N(CH_3)_4^+ > NH_4^+ > Cs^+ > Rb^+ > K^+ > Na^+ > Li^+ > Ca^{2+} > Mg^{2+}$. However, the mechanism driving the salting-in−salting-out behavior in this series is not fully understood. Studies based on small solutes such as butyramide and macromolecules like poly(*N*-isopropylacrylamide) (PNIPAM) as well as proteins have indicated that weakly hydrated monovalent cations tend to be depleted from the solute whereas strongly hydrated divalent cations interact weakly with the amide moiety.[2,5,11] Bruce et al.[5] proposed a salting-in contribution due to the interaction of Ca^{2+} and $CaCl^+$ solvent-shared ion pairs with the amide oxygen based on a combination of cloud point experiments and MD simulations. However, the cumulative effect of all the interactions still led to net salting-out behavior for PNIPAM. Understanding these ion effects on the conformations of macromolecules is imperative, particularly in the case of intrinsically disordered proteins (IDPs) whose aggregation is believed to play an important role in neurodegenerative diseases.[12−15] The binding of ions, especially multivalent cations, with IDPs may promote/inhibit chain conformations which may accelerate the formation of neurotoxic aggregates,[13,15] which motivates us to provide atomistic insight into cation−IDP interactions. To that end, we consider a typical IDP-like model system, the elastin-like polypeptides (ELPs).[16] The ELPs are pentameric repeats of VPGXG, whereby X represents different combinations of G, A, and V in the fourth position. We study the phase behavior of two ELP sequences, namely, V_5-120 and $V_5A_2G_3$-120 (where 120 represents the total number of pentamers per ELP chain) in chloride salts of divalent cations, Ca^{2+} and Mg^{2+}. ELPs exhibit a lower critical solution temperature (LCST) transition in aqueous solutions with an expanded−collapsed conformational change.[17−19] The cloud point of ELPs depends on the guest residue, the molecular weight, salts, and other cosolvents.[17,20−28] Significantly, we observe that the Mg^{2+}−amide oxygen interaction can lead to salting-out (V_5) or salting-in ($V_5A_2G_3$) behavior at a high salt concentration. By contrast, Ca^{2+}−amide oxygen bridging interactions lead to salting-out of both V_5 and $V_5A_2G_3$. Molecular dynamics simulations show that the effect of divalent salts on the phase behavior of ELPs is mainly determined by a competition between the cation−amide oxygen and the cation−hydration water interactions. Additionally, the ionic interactions are strongly influenced by the presence of triglycine motifs (pentamers with G as guest residues).

Figure 1 depicts the molecular mechanism for the observed salt effects on the phase behavior of ELPs derived from atomistic molecular dynamics simulations, thermodynamic measurements, and infrared spectroscopy. The divalent cations, Ca^{2+} and Mg^{2+}, interact weakly with the amide oxygens (it should be noted that most of the cations are depleted from the ELP chain). Ca^{2+} cations are able to shed

Received: September 4, 2023
Revised: October 16, 2023
Accepted: October 24, 2023
Published: November 3, 2023

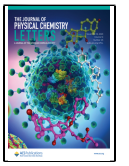

https://doi.org/10.1021/acs.jpclett.3c02476
J. Phys. Chem. Lett. 2023, 14, 10113−10118

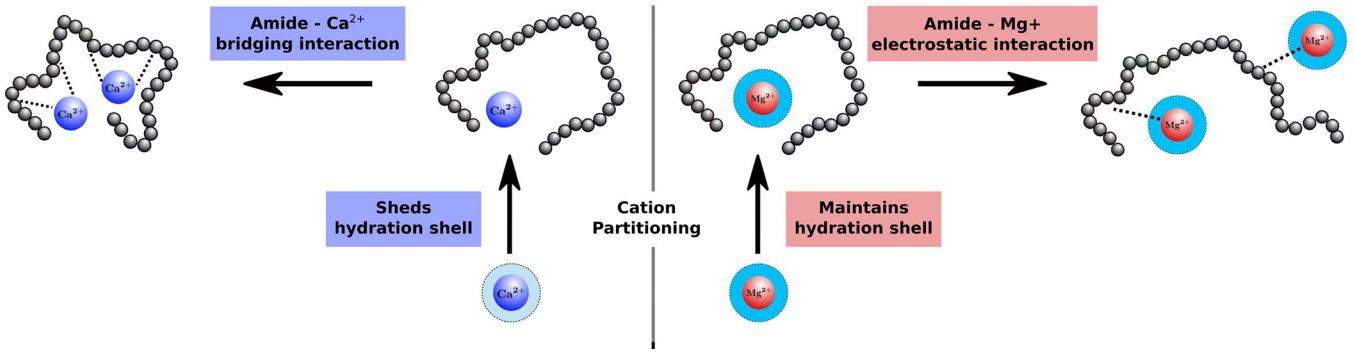

Figure 1. Schematic illustration of the interaction between two divalent cations, Ca^{2+} and Mg^{2+}, and ELPs, as derived from molecular dynamics simulations, thermodynamic measurements, and infrared spectroscopy.

their hydration shell water molecules and engage in the formation of ion bridges among two amide oxygen atoms. This mechanism leads to a rapidly decreasing cloud point temperature (salting-out). On the other hand, Mg^{2+} cations bind their hydration water tightly as compared to Ca^{2+}. As a result, the Mg^{2+} ions partition to the ELP chain along with their hydration waters and are therefore not able to form ion bridges. The partitioning of the hydrated Mg^{2+} cations to the ELP chain increases with increasing salt concentration, which leads to the salting-in of the ELP at higher salt concentrations. Moreover, the triglycine motifs in $V_5A_2G_3$ (which makes the polymer chain more flexible and less hydrophobic compared with V_5) are revealed to play a significant role in regulating the phase behavior of ELPs in salt solutions.

Phase Behavior of ELPs in Aqueous Salt Solutions. The top panel of Figure 2 shows the cloud point temperature of two 120 pentamer repeat ELP sequences, $V_5A_2G_3$-120 and V_5-120 (5 mg/mL of each ELPs), in $CaCl_2$ and $MgCl_2$ solutions. Readers are referred to Section S1 in the Supporting Information for details pertaining to the materials and experiments. For c < 1.5 M, the cloud point temperature decreases with increasing salt concentration, indicating the salting-out effect of $CaCl_2$ with both ELPs. At $CaCl_2$ concentrations above c > 1.5 M, the cloud point of both ELPs decreases sharply with increasing salt concentration. Interestingly, the two ELPs have different phase behaviors in the $MgCl_2$ solution. $V_5A_2G_3$ showed salting-out behavior (decreasing cloud point) at low $MgCl_2$ concentration (c < 1.5 M), but salting-in behavior (increasing cloud point) was observed at high $MgCl_2$ concentration (c > 1.5 M); see Figure 2a. By contrast, the cloud point of V_5 monotonically decreased with increasing salt concentration at both low and high $MgCl_2$ concentration; see Figure 2b. Therefore, $MgCl_2$ had a similar effect as $CaCl_2$ on the phase behavior of V_5, albeit the cloud point decreased to a smaller extent in the solution with $MgCl_2$. Two key observations from Figure 2 are the effect of divalent metal salts on the phase behavior of ELPs is (a) cation-specific and salt concentration dependent and (b) sequence dependent. The difference between the cloud point behavior of the two ELPs in divalent metal salt solutions is likely caused by the presence of flexible triglycine motifs in $V_5A_2G_3$.

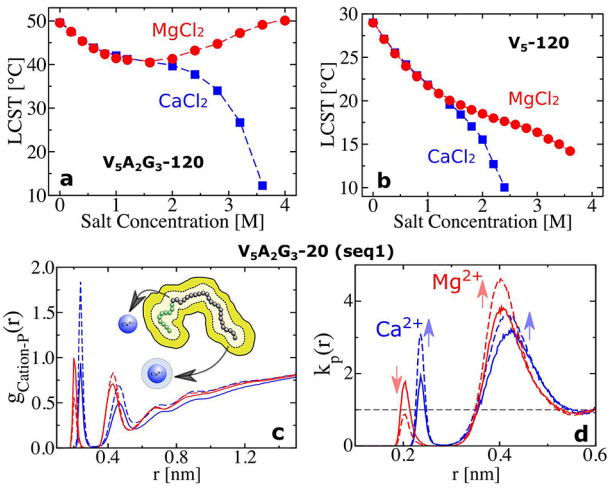

Figure 2. Top Panel: The cloud point temperature of (a) $V_5A_2G_3$-120 and (b) V_5-120 in $MgCl_2$ and $CaCl_2$ solutions as a function of salt concentration. Note, the unit M represents the molar concentration of salt. Bottom Panel: The variation of the (c) cation and amide oxygen radial distribution function, $g(r)$, and (d) the partition coefficient, $k_p(r)$, with r, which corresponds to the proximal cation/water−amide oxygen distance for seq1 from molecular dynamics simulations. For the bottom panel, the solid and dashed blue lines show the data in $CaCl_2$ at 1.0 and 2.5 M, respectively, and the solid and dashed red lines are the results in $MgCl_2$ at 1.0 and 2.5 M, respectively.

ELP−Cation Interactions. To understand the mechanisms governing the observations in Figure 2a, we studied the interactions of Ca^{2+} and Mg^{2+} with two 20 pentamer repeat ELP sequences, $G_6A_4V_{10}$ (seq1) and $G_3A_2V_{10}A_2G_3$ (seq2), using atomistic molecular dynamics (MD) simulations at two salt concentrations, 1.0 and 2.5 M. In seq1, the flexible tryglycine motifs (pentamers with G as the guest residue, VPGGG) are placed in one block of the ELP chain (G_6 on one terminus). By contrast, in seq2, the tryglycine motifs are placed on either end of the ELP chain (G_3 on both terminals). For each salt concentration, the averaged thermodynamic properties were computed from 3 independent 1 μs simulation trajectories, which sufficiently sampled the conformational ensemble of the ELP chain. Details pertaining to the force fields and simulations can be found in Section S2, Figures S1 and S2, and Table S1 in the Supporting Information. The two sequences were studied to investigate the role of triglycine motifs. The change in the gyration radius of the ELP chain with increasing salt concentration from the MD simulations (Figure S3 for more details) agreed with the cloud point trends observed in Figure 2. Previous simulation studies involving PNIPAM in aqueous $CaCl_2$ solutions have shown that the divalent cations locally accumulate around the amide oxygen.[5] Given this observation, we examined the distribution of divalent cations around the amide oxygen atoms of the ELPs.

https://doi.org/10.1021/acs.jpclett.3c02476
J. Phys. Chem. Lett. 2023, 14, 10113−10118

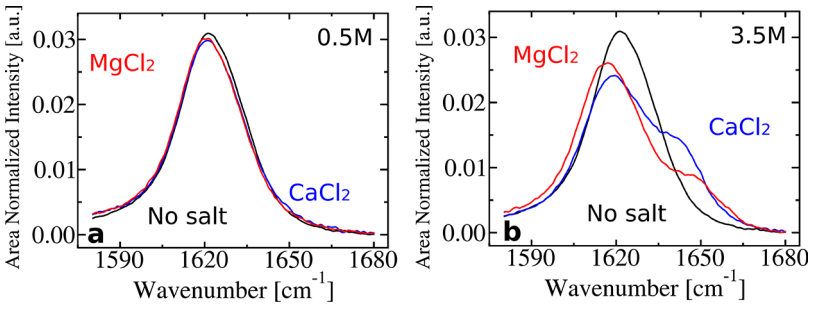

Figure 3. Infrared spectra of NMA at 0.5 M (a) and 3.5 M (b) salt concentration. The black line shows the data in pure D_2O water, and the red and blue lines are the results for $MgCl_2$ and $CaCl_2$, respectively.

Figure 2c shows the radial distribution function (rdf) between the amide oxygen (OA) of seq1 and the divalent cations (M^{2+}). The first and second peaks of rdf can be attributed to contact OA−M^{2+} and solvent-separated OA−M^{2+} interactions, respectively. The data indicate that Ca^{2+} ions, shown in blue, shed their hydration waters and interacted more strongly with the amide oxygen atoms via contact interactions than via solvent-separated interactions. Moreover, the Ca^{2+} ions were engaged in bridging interactions involving two amide oxygen atoms (a snapshot of the formed Ca^{2+} bridge can be seen in Figure S4 in the Supporting Information). The formation of these Ca^{2+}-ion bridges provides an explanation for why the LCST data shown in Figure 2a fell rapidly as a function of the $CaCl_2$ concentration, especially at high salt concentrations. Quantitative analysis indicated that the Ca^{2+} bridging interactions involved a combination of local (bridged oxygen atoms (i, j) less than three amino acid residues away, $|i - j| \leq 2$) and global ($|i - j| > 2$) bridging contacts, but most bridging interactions were local. The fraction of the global Ca^{2+} bridges grew slightly at higher salt concentration but a more pronounced increase was observed for the maximum bridging range ($|i - j|_{max} = 99$ at 2.5 M; see Section S3 and Tables S2 and S3 for more details).

In contrast to Ca^{2+} ions, Mg^{2+} cations preferred to engage in solvent-separated interactions with the amide oxygen atoms (see red curves in Figure 2c), and thus no Mg^{2+} bridges were formed. This observation can be attributed to the fact that Mg^{2+} cations are strongly hydrated and bind their hydration waters tighter than Ca^{2+} cations.[29,30] With increasing $MgCl_2$ concentration, the number of contact OA−Mg^{2+} interactions decreased, whereas the number of solvent separated interactions increased. This occurs due to the tendency of Mg^{2+} ions to maximize their favorable electrostatic interactions with amide oxygen atoms without shedding their hydration shell water molecules. This enhanced partitioning of Mg^{2+} along with their hydration waters explains the salting-in of the ELP at high $MgCl_2$ concentrations (Figure 2a).

The different effects of the two divalent cations were also observed in the local bulk partition coefficient $k_p(r)$ values as a function of position (see eq S6 in the Supporting Information). This quantity has the property $k_p(r) > 1$ when cations partition more favorably than water to the ELP chain, while $k_p(r) < 1$ (cations are depleted) in the opposite scenario. As such, $k_p(r)$ provides a measure of the ion-to-water affinity. Figure 2d, shows that with increasing salt concentration, Ca^{2+} preferably accumulated in the contact OA−Ca^{2+} shell (first peak) whereas Mg^{2+} ions tended to preferably accumulate in the solvent shared OA−Ca^{2+} shell (second peak), leading to the contrasting behavior observed in Figure 2c. For seq2, identical trends were observed, as shown in Figure S5 in the Supporting Information. Therefore, the effect of divalent cations on the phase behavior of ELPs can be explained as a competition between the nature of the cation−amide oxygen electrostatic interactions (contact interactions and bridges) and the strength of cation hydration (solvent-shared interactions). This mechanism explains the different cloud point temperature trends for ELP $V_5A_2G_3$ shown in Figure 2a.

We have also calculated the number of cation−chloride contact ion pairs (CIPs) and solvent-shared ion pairs (SIPs) in salt solutions without the ELP. The results are shown in Figure S6 in the Supporting Information. As the salt concentration increased, the absence of Mg^{2+}−Cl^- CIPs and the increasing number of Mg^{2+}−Cl^- SIPs further verified our observation that Mg^{2+} ions bound their hydration waters tightly. By contrast, the progressively growing number of Ca^{2+}−Cl^- CIPs confirmed that Ca^{2+} cations shed their hydration shells. Bruce et al. have shown that the partitioning of the Ca^{2+}−Cl^- SIPs to PNIPAM provided a salting-in contribution to the polymer chain.[5] Our analysis of cation−chloride SIPs in ELP solutions (Figure S7 in the Supporting Information) suggested that a similar contribution may be present in the case of ELPs in $MgCl_2$ solution: the increased number of Mg^{2+}−Cl^- SIPs in the solvation shell of the ELP correlated with the salting-in of the ELP at high $MgCl_2$ concentrations. In contrast to Mg^{2+}, the increased number of Ca^{2+}−Cl^- CIPs correlated with the salting-out of the ELP at high $CaCl_2$ concentrations. This suggests that the salting-out contribution due to bridging provided by Ca^{2+}−Cl^- CIPs overcompensated for the salting-in contribution provided by the Ca^{2+}−Cl^- SIPs (see the Supporting Information for more details).

Amide Oxygen−Cation Pairing and Infrared Spectroscopy. The inferences obtained from the MD simulations can be experimentally confirmed by infrared spectroscopy, which can be used to detect the presence of ELP amide oxygen−cation contact and solvent-shared shells by monitoring the amide I band. However, the amide I band for ELPs is highly dependent on the hydrogen bonding network of the amide oxygen and susceptible to the changes in secondary structures of the ELPs (see Figure S8 in the Supporting Information). To avoid this problem, we used *N*-methylacetamide (NMA) as a model system instead. It has no secondary structures and thus changes to its amide I band in salt solutions were caused by perturbation of the hydration shell via interactions with the ions. The infrared spectra of NMA with $CaCl_2$ and $MgCl_2$ are shown in Figure 3. One can be seen that the spectra of NMA in 0.5 M $CaCl_2$ or $MgCl_2$ solutions are very similar to pure D_2O water (Figure 3a). This changes at 3.5 M salt. The main resonance at 1622 cm^{-1} in neat D_2O red shifts to 1617.4 and

https://doi.org/10.1021/acs.jpclett.3c02476
J. Phys. Chem. Lett. 2023, 14, 10113−10118

1619.5 cm^{-1} for $MgCl_2$ and $CaCl_2$, respectively. This red shift has previously been assigned[31] to a local electric field along the dipole of the amide (Figure 3b). Herein, this peak is assigned to the cation−amide oxygen solvent-separated interactions and is larger for Mg^{2+}. The second peak centered at 1649.0 cm^{-1} for Mg^{2+} and 1647.1 cm^{-1} for Ca^{2+} grows with higher salt concentrations and is assigned to the cation−amide oxygen contact interactions. A smaller quantity of contact interactions is observed for Mg^{2+}, which is consistent with the all-atom simulation results.

Role of Triglycine Motifs. The top and middle panels of Figure 4 compare the rdf of M^{2+} with the whole ELP chain to the rdf

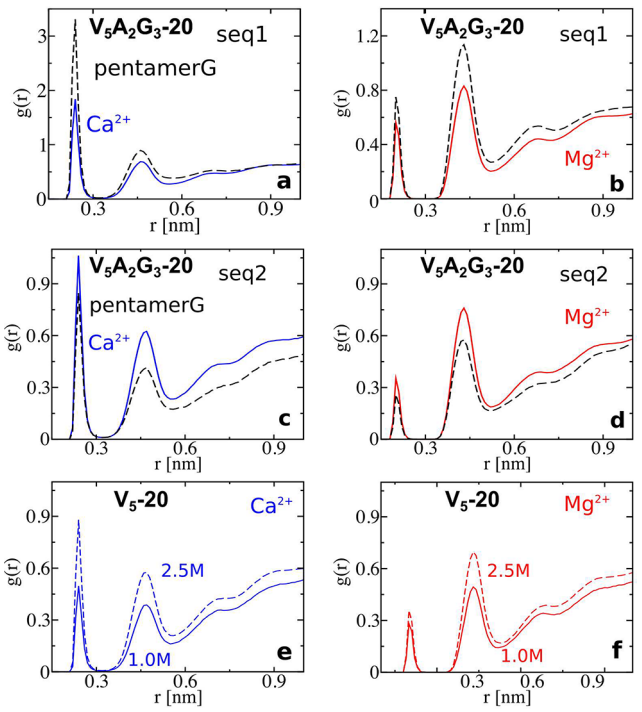

Figure 4. Top and Middle Panels: Comparison of the radial distribution function $g(r)$ between the whole chain (solid lines) and pentamerG (dashed lines) for the ELP $V_5A_2G_3$ 20-mer at a 2.5 M salt concentration. Plots (a) and (b) are for seq1 in $CaCl_2$ and $MgCl_2$ solutions, respectively. Plots (c) and (d) are the same as plots (a) and (b) but for seq2. Data at 1.0 M salt concentration can be found in Figure S9 in the Supporting Information. Bottom Panel: M^{2+}−ELP rdf of the V_5 20-mer. Plots (e) and (f) are the results for Ca^{2+} and Mg^{2+}, respectively. The solid and dashed lines are for 1.0 and 2.5 M, respectively.

of M^{2+} with only the pentamerG (-(VPGGG)- tryglycine motifs) units of the ELP chain for seq1 and seq2. For seq1 (see Figure 4a,b), both Ca^{2+} and Mg^{2+} preferentially partitioned to the segments with triglycine motifs as the first and second peak intensities of the rdf for M^{2+}−pentamerG are larger than the M^{2+}−ELP rdf. On the other hand, the partitioning of the M^{2+} ions to the triglycine motifs of seq2 was lower than the rest of the chain (see Figure 4c,d). Additionally, the overall partitioning of the divalent cations to seq2 was lower than that of seq1 at both considered salt concentrations. Seq1 has a long flexible terminus, in comparison to seq2, as all segments with triglycine motifs (which are very flexible) have been placed in one block. The presence of this single long flexible terminus in seq1 allows for conformations that may lead to an efficient interaction between the divalent cations and the amide oxygen atoms as compared to seq2. This is supported by the observation that more Ca^{2+} bridges were found within pentamerG segments in seq1 in comparison to seq2 (see Table S3 in the Supporting Information). This shows that both the location and the length of the triglycine motifs play important roles in regulating ELP−cation interactions for 20-mer ELP chains.

The bottom panel of Figure 4 shows the M^{2+}−ELP rdf for the more hydrophobic and less flexible V_5 20-mer in $CaCl_2$ and $MgCl_2$ solutions. The peak intensities of the M^{2+}−ELP rdfs for the V_5 20-mer were smaller than those for seq2 at both salt concentrations that were considered (note that the M^{2+}−ELP rdfs for seq2 are much smaller than seq1). This observation further supports our conclusion that triglycine motifs enhanced ELP−cation interactions.

We have shown that the phase behavior of two ELPs, $V_5A_2G_3$ and V_5, in solution with divalent metal cations is regulated by a competition between amide oxygen−cation electrostatic interactions and the strength of cation hydration. The divalent cation, Ca^{2+}, was able to shed its hydration shell and bridge two amide−oxygen atoms together, leading to the salting-out of ELPs, which was far more enhanced at higher salt concentrations. By contrast, Mg^{2+} interacted predominantly with the amide oxygen atoms via solvent-separated electrostatic interactions that led to a salting-in effect for ELP $V_5A_2G_3$-120 at high salt concentrations. Moreover, the presence of triglycine motifs was found to regulate the phase behavior of ELPs as evidenced by the different LCST behaviors of $V_5A_2G_3$ and V_5 (with and without triglycine motifs) in $MgCl_2$ and $CaCl_2$ solutions.

Although the contrasting effects of Ca^{2+} and Mg^{2+} on the phase behavior of these two ELPs are present only at molar salt concentrations, analogous Ca^{2+} bridging behavior occurs at physiological salt concentrations with charged carboxylate residues. An in vivo example of this concerns the EF Hand motif in Ca^{2+} binding proteins.[32] Also, Bilkov et al. have shown that the preferential bridging of phosphate moieties by Ca^{2+} over Mg^{2+} can inhibit the binding of PH Domains to PI(4,5)P2 lipids in biomembranes.[33] It would therefore seem that the bridging of protein sites in water is a common characteristic of Ca^{2+} over Mg^{2+} with a number of different chemistries. Additionally, it is possible that direct physiological implications of the Ca^{2+} bridging of amide oxygens might occur under exceptionally high salt concentrations such as in the Dead Sea in Israel (1.65 M Ca^{2+} and 0.42 M Mg^{2+}) or in the Don Juan Pond in Antarctica (4.1 M Ca^{2+} and 0.1 M Mg^{2+}).[34−37]

■ ASSOCIATED CONTENT

Supporting Information

The Supporting Information is available free of charge at https://pubs.acs.org/doi/10.1021/acs.jpclett.3c02476.

Experimental details, simulation details (force field parameters (Table S1), derivative of activity coefficients vs concentration and PMF (Figures S1 and S2)), tables of backbone separation $|i - j|$ of Ca^{2+} ion bridges (Table S2), fraction of Ca^{2+} ion bridges in pentamerG (Table S3), Gyration radius as a function of salt concentration (Figure S3), calcium ion bridges (Figure S4), radial distribution function and k_p for seq2 (Figure S5), radial distribution function for cation−chloride pairing (Figure S6), cumulative number cation−chloride pairing (Figure

https://doi.org/10.1021/acs.jpclett.3c02476
J. Phys. Chem. Lett. 2023, 14, 10113−10118

S7), infrared spectra of $V_5A_2G_3$ (Figure S8), triglycine motif effects (Figure S9) (PDF)

AUTHOR INFORMATION

Corresponding Authors

Paul S. Cremer − *Department of Chemistry and Department of Biochemistry and Molecular Biology, Penn State University, University Park, Pennsylvania 16802, United States;* orcid.org/0000-0002-8524-0438; Email: psc11@psu.edu

Nico F. A. van der Vegt − *Department of Chemistry, Technical University of Darmstadt, 64287 Darmstadt, Germany;* orcid.org/0000-0003-2880-6383; Email: vandervegt@cpc.tu-darmstadt.de

Authors

Yani Zhao − *Department of Chemistry, Technical University of Darmstadt, 64287 Darmstadt, Germany;* orcid.org/0000-0003-1430-4518

Swaminath Bharadwaj − *Department of Chemistry, Technical University of Darmstadt, 64287 Darmstadt, Germany; Department of Chemical Engineering, Shiv Nadar Institution of Eminence, Gautam Buddha Nagar, Uttar Pradesh 201314, India;* orcid.org/0000-0002-6875-3506

Ryan L. Myers − *Department of Chemistry, Penn State University, University Park, Pennsylvania 16802, United States*

Halil I. Okur − *Department of Chemistry, Penn State University, University Park, Pennsylvania 16802, United States;* orcid.org/0000-0002-2492-1168

Pho T. Bui − *Department of Chemistry, Penn State University, University Park, Pennsylvania 16802, United States;* orcid.org/0000-0003-2722-5982

Mengrui Cao − *Department of Chemistry, Penn State University, University Park, Pennsylvania 16802, United States*

Lauren K. Welsh − *Department of Chemistry, Penn State University, University Park, Pennsylvania 16802, United States*

Tinglu Yang − *Department of Chemistry, Penn State University, University Park, Pennsylvania 16802, United States;* orcid.org/0000-0003-0872-8218

Complete contact information is available at: https://pubs.acs.org/10.1021/acs.jpclett.3c02476

Author Contributions

[‖]Y.Z., S.B., and R.L.M. contributed equally to this work.

Notes

The authors declare no competing financial interest.

ACKNOWLEDGMENTS

Y.Z. and N.F.A.v.d.V. acknowledge funding from Deutsche Forschungsgemeinschaft (DFG) through the Collaborative Research Center Transregio TRR 146 Multiscale Simulation Methods for Soft Matter Systems. R.L.M. and P.S.C. acknowledge funding from the National Science Foundation (NSF), CHE-2305129 and CHE-2004050. S.B. acknowledges financial assistance provided by the Ministry of Education, India through SERB, India (SRG/2023/000202).

REFERENCES

(1) Schneider, C. P.; Shukla, D.; Trout, B. L. Arginine and the Hofmeister Series: The Role of Ion−Ion Interactions in Protein Aggregation Suppression. *J. Phys. Chem. B* **2011**, *115*, 7447−7458.

(2) Okur, H. I.; Hladílková, J.; Rembert, K. B.; Cho, Y.; Heyda, J.; Dzubiella, J.; Cremer, P. S.; Jungwirth, P. Beyond the Hofmeister Series: Ion-Specific Effects on Proteins and Their Biological Functions. *J. Phys. Chem. B* **2017**, *121*, 1997−2014.

(3) Jungwirth, P.; Cremer, P. S. Beyond Hofmeister. *Nat. Chem.* **2014**, *6*, 261−263.

(4) Bruce, E. E.; Bui, P. T.; Rogers, B. A.; Cremer, P. S.; van der Vegt, N. F. A. Nonadditive ion effects drive both collapse and swelling of thermoresponsive polymers in water. *J. Am. Chem. Soc.* **2019**, *141*, 6609−6616.

(5) Bruce, E. E.; Okur, H. I.; Stegmaier, S.; Drexler, C. I.; Rogers, B. A.; van der Vegt, N. F. A.; Roke, S.; Cremer, P. S. Molecular mechanism for the interactions of Hofmeister cations with macromolecules in aqueous solution. *J. Am. Chem. Soc.* **2020**, *142*, 19094−19100.

(6) Zhao, Y.; Bharadwaj, S.; van der Vegt, N. F. A. Nonadditive ion effects on the coil−globule equilibrium of PNIPAM: a computer simulation study. *Phys. Chem. Chem. Phys.* **2022**, *24*, 10346−10355.

(7) Hofmeister, F. Zur Lehre von der Wirkung der Salze. *Arch. Exp. Pathol. Pharm.* **1888**, *25*, 1−30.

(8) Kunz, W.; Henle, J.; Ninham, B. 'Zur Lehre von der Wirkung der Salze' (about the science of the effect of salts): Franz Hofmeister's historical papers. *Curr. Opin. Colloid Interface Sci.* **2004**, *9*, 19−37.

(9) Baldwin, R. How Hofmeister ion interactions affect protein stability. *Biophys. J.* **1996**, *71*, 2056−2063.

(10) Clarke, R. J.; Lüpfert, C. Influence of Anions and Cations on the Dipole Potential of Phosphatidylcholine Vesicles: A Basis for the Hofmeister Effect. *Biophys. J.* **1999**, *76*, 2614−2624.

(11) Okur, H. I.; Kherb, J.; Cremer, P. S. Cations Bind Only Weakly to Amides in Aqueous Solutions. *J. Am. Chem. Soc.* **2013**, *135*, 5062−5067.

(12) Uversky, V. N. Targeting intrinsically disordered proteins in neurodegenerative and protein dysfunction diseases: another illustration of the D2 concept. *Expert Rev. Proteomics* **2010**, *7*, 543−564.

(13) Breydo, L.; Uversky, V. N. Role of metal ions in aggregation of intrinsically disordered proteins in neurodegenerative diseases. *Metallomics* **2011**, *3*, 1163−1180.

(14) Uversky, V. N. Intrinsically disordered proteins and their (disordered) proteomes in neurodegenerative disorders. *Front. Aging Neurosci.* **2015**, *7*, 00018.

(15) Matsarskaia, O.; Roosen-Runge, F.; Schreiber, F. Multivalent ions and biomolecules: Attempting a comprehensive perspective. *ChemPhysChem* **2020**, *21*, 1742−1767.

(16) Roberts, S.; Dzuricky, M.; Chilkoti, A. Elastin-like polypeptides as models of intrinsically disordered proteins. *FEBS Lett.* **2015**, *589*, 2477−2486.

(17) Urry, D. W.; Gowda, D. C.; Parker, T. M.; Luan, C.-H.; Reid, M. C.; Harris, C. M.; Pattanaik, A.; Harris, R. D. Hydrophobicity scale for proteins based on inverse temperature transitions. *Biopolymers* **1992**, *32*, 1243−1250.

(18) Urry, D. W. Physical Chemistry of Biological Free Energy Transduction As Demonstrated by Elastic Protein-Based Polymers. *J. Phys. Chem. B* **1997**, *101*, 11007−11028.

(19) Roberts, S.; Dzuricky, M.; Chilkoti, A. Elastin-like polypeptides as models of intrinsically disordered proteins. *FEBS Lett.* **2015**, *589*, 2477−2486.

(20) Meyer, D. E.; Chilkoti, A. Genetically Encoded Synthesis of Protein-Based Polymers with Precisely Specified Molecular Weight and Sequence by Recursive Directional Ligation: Examples from the Elastin-like Polypeptide System. *Biomacromolecules* **2002**, *3*, 357−367.

(21) Meyer, D. E.; Chilkoti, A. Quantification of the Effects of Chain Length and Concentration on the Thermal Behavior of Elastin-like Polypeptides. *Biomacromolecules* **2004**, *5*, 846−851.

(22) Cho, Y.; Zhang, Y.; Christensen, T.; Sagle, L. B.; Chilkoti, A.; Cremer, P. S. Effects of Hofmeister Anions on the Phase Transition Temperature of Elastin-like Polypeptides. *J. Phys. Chem. B* **2008**, *112*, 13765−13771.
(23) Ribeiro, A.; Arias, F. J.; Reguera, J.; Alonso, M.; Rodríguez-Cabello, J. C. Influence of the Amino-Acid Sequence on the Inverse Temperature Transition of Elastin-Like Polymers. *Biophys. J.* **2009**, *97*, 312−320.
(24) Rembert, K. B.; Paterová, J.; Heyda, J.; Hilty, C.; Jungwirth, P.; Cremer, P. S. Molecular Mechanisms of Ion-Specific Effects on Proteins. *J. Am. Chem. Soc.* **2012**, *134*, 10039−10046.
(25) Heyda, J.; Okur, H. I.; Hladílková, J.; Rembert, K. B.; Hunn, W.; Yang, T.; Dzubiella, J.; Jungwirth, P.; Cremer, P. S. Guanidinium can both Cause and Prevent the Hydrophobic Collapse of Biomacromolecules. *J. Am. Chem. Soc.* **2017**, *139*, 863−870.
(26) Zhao, Y.; Kremer, K. Proline isomerization regulates the phase behavior of elastin-like polypeptides in water. *J. Phys. Chem. B* **2021**, *125*, 9751−9756.
(27) Zhao, Y.; Singh, M. K.; Kremer, K.; Cortes-Huerto, R.; Mukherji, D. Why Do Elastin-Like Polypeptides Possibly Have Different Solvation Behaviors in Water-Ethanol and Water-Urea Mixtures? *Macromolecules* **2020**, *53*, 2101−2110.
(28) Mills, C. E.; Ding, E.; Olsen, B. D. Cononsolvency of Elastin-like Polypeptides in Water/Alcohol Solutions. *Biomacromolecules* **2019**, *20*, 2167−2173.
(29) Bleuzen, A.; Pittet, P.-A.; Helm, L.; Merbach, A. E. Water exchange on magnesium(II) in aqueous solution: a variable temperature and pressure 17O NMR study. *Magn. Reson. Chem.* **1997**, *35*, 765−773.
(30) Helm, L.; Merbach, A. Water exchange on metal ions: experiments and simulations. *Coord. Chem. Rev.* **1999**, *187*, 151−181.
(31) Drexler, C. I.; Cracchiolo, O. M.; Myers, R. L.; Okur, H. I.; Serrano, A. L.; Corcelli, S. A.; Cremer, P. S. Electric Fields in Aqueous Electrolytes. *J. Phys. Chem. B* **2021**, *125*, 8484−8493.
(32) Gifford, J.; Walsh, M.; Vogel, H. Structures and metal-ion-binding properties of the Ca2+-binding helix−loop−helix EF-hand motifs. *Biochem. J.* **2007**, *405*, 199−221.
(33) Bilkova, E.; Pleskot, R.; Rissanen, S.; Sun, S.; Czogalla, A.; Cwiklik, L.; Róg, T.; Vattulainen, I.; Cremer, P. S.; Jungwirth, P.; Coskun, Ü. Calcium Directly Regulates Phosphatidylinositol 4,5-Bisphosphate Headgroup Conformation and Recognition. *J. Am. Chem. Soc.* **2017**, *139*, 4019−4024.
(34) Nissenbaum, A. Minor and trace elements in Dead Sea water. *Chem. Geol.* **1977**, *19*, 99−111.
(35) Nissenbaum, A. The microbiology and biogeochemistry of the Dead Sea. *Microb. Ecol.* **1975**, *2*, 139−161.
(36) Toner, J.; Catling, D.; Sletten, R. The geochemistry of Don Juan Pond: Evidence for a deep groundwater flow system in Wright Valley, Antarctica. *Earth Planet. Sci. Lett.* **2017**, *474*, 190−197.
(37) Siegel, B. Z.; Mcmurty, G.; Siegel, S. M.; Chen, J.; Larock, P. Life in the calcium chloride environment of Don Juan Pond, Antarctica. *Nature* **1979**, *280*, 828−829.

https://doi.org/10.1021/acs.jpclett.3c02476
J. Phys. Chem. Lett. 2023, 14, 10113−10118